Asymmetric Cellulose Acetate Hollow Fibers: Studies in Gas Permeation

Gas separation behavior of permeators containing asymmetric cellulose acetate hollow fibers with the dense skin on the outside, facing the feed gas, has been investigated experimentally and theoretically using a sweep gas technique. Two systems were studied: CO_2-N_2, and O_2-N_2 (air). If the membrane structure is assumed to be symmetric or homogeneous, the model complies with the present data much better, compared to the assumption that the membrane is asymmetric.

Separation was carried out with the high-pressure feed outside the fibers as well as inside the fibers. In both cases the data were well predicted by the homogeneous model. No concentration polarization effects were found when the feed flowed inside the fibers. The inherent membrane separation capability appeared practically the same whether the feed was inside or outside the fibers. Internal pressurization did not damage the membrane performance for the low pressure range used.

These findings enable the operation of asymmetric hollow-fiber permeators with the feed inside the fiber lumen, which gives better separation in high stage cut situations.

M. Sidhoum, A. Sengupta, K. K. Sirkar
Department of Chemistry and Chemical Engineering
Stevens Institute of Technology
Castle Point, Hoboken, NJ 07030

Introduction

Large-scale membrane gas separation devices invariably use asymmetric membranes to achieve the desired combination of high-permeation flux and selectivity (Bollinger et al., 1982; Mazur and Chan, 1982; Schell and Houston, 1982; Yamashiro et al., 1984; Pan, 1983, 1986). Understanding the separation behavior of such membranes is therefore of considerable importance. If the asymmetric membrane is modeled as a combination of (1) an ultrathin dense skin wherein lies all the permeation resistance, and (2) a very porous support layer that offers no permeation resistance but creates a crossflow pattern in the membrane, then the permeation equations will be different from those for a homogeneous (symmetric) membrane (Pan 1983, 1986). Other modeling efforts involving asymmetric membranes have followed the same idealized assumption (Sengupta and Sirkar, 1986, 1987; Perrin and Stern, 1986).

In a recent investigation (Sengupta and Sirkar, 1987), it was found that the behavioral pattern of a supposedly asymmetric membrane did not quite follow the ideal asymmetric membrane model described above. In the above study, the experimental performance of an asymmetric cellulose acetate (CA) hollow-fiber permeator was compared with the theoretical predictions based on an asymmetric membrane model, and also with the theoretical predictions based on the usual homogeneous membrane model. In most cases it was not possible to conclude unequivocally that the asymmetric membrane model fitted the data better. This was observed for binary (CO_2-N_2) as well as ternary (He-CO_2-N_2) systems, for pressures up to 5 atm, and over a wide range (up to 60%) of stage cuts. The pure-component permeabilities, measured *in situ* in the permeator itself, were used in the simulations. The basic assumption is that the permeation rate per unit driving force is the same for the two models.

We have undertaken the present study to explore in depth the gas separation behavior of the supposedly asymmetric CA hollow fibers vis-a-vis the homogeneous model and the asymmetric model. This has been done using a sweep gas technique, whereby the difference between the two models can be enhanced considerably. As a result, it becomes easier to determine which model predicts the actual experimental behavior better. This mode of operation with sweep gas is of interest in itself for those gas sepa-

Correspondence concerning this paper should be addressed to K.K. Sirkar.

ration situations where driving force maximization is necessary in the absence of a high-pressure feed (Pan and Habgood, 1974). Two systems have been studied: CO_2-N_2 and O_2-N_2 (air).

If the CA fiber behaves more as a homogeneous membrane what are its implications? Could one use the high-pressure feed gas inside the fiber? Generally, asymmetric hollow fibers for gas separation have the dense skin on the outside. Therefore, in practice the high-pressure feed flows on the outside of the fiber, called here the feed-outside mode. This approach is also followed for composite hollow fibers as in PRISM separators with silicone rubber coated asymmetric polysulfone hollow fibers (Henis and Tripodi, 1980, 1981). However, should these hollow fibers behave essentially as a homogeneous membrane for separation, it may be possible to let the feed gas mixture flow through the fiber lumen instead, collecting the permeate from outside the fibers. Such a reversed feed, or feed-inside, mode of operation is known to be advantageous for high stage cut operation in homogeneous hollow-fiber permeators (Antonson et al., 1977; Pan and Habgood, 1978). Note that homogeneous silicone capillary permeators have been operated in both modes (Blaisdell and Kammermeyer, 1973; Stern et al., 1977).

We have therefore investigated here the performance of the feed-inside mode under various conditions. The pure-component permeabilities for the CA fibers were measured under the feed-inside configuration also. Using the above permeabilities, simulations were carried out assuming the fibers to be essentially homogeneous, and results were compared with data to check how well the homogeneous membrane model is applicable to the feed-inside mode. The permeator performances in the feed-inside and in the feed-outside mode were also compared under identical feed pressure conditions.

There are two other aspects of importance in the present study regarding the reversed feed mode: concentration polarization and hysteresis. For the first, it is of interest to determine the effects, if any, of concentration polarization in the porous support layer in contact with the feed gas mixture. A reversed mode of operation is known to be highly detrimental to liquid separations such as reverse osmosis, (RO) due to concentration polarization (Mehta and Loeb, 1978) even though a different conclusion has been reached for pervaporation (Rautenbach and Albrecht, 1984).

Second, in the feed-inside mode, the fiber lumen is pressurized. The dense skin no longer has the mechanical support of the porous backing. Even though CA is a stiff polymer, it is possible that the pressurization may cause some irreversible compaction and structural change in the porous support layer; defects may develop in the skin resulting in subsequent change of performance in the normal or feed-outside mode. In the present investigations, studies were made to see if indeed there is such hysteresis-type performance change for the pressure range employed. It is believed that such studies will generate a better understanding of the nature of the asymmetric membrane structure and provide its efficient utilization in a broader framework of hollow-fiber gas separators.

Theory

Feed-outside mode/shell-side feed

For permeation of a pure species in a hollow-fiber permeator with high-pressure feed on the outside, the permeation rate across a differential length dl can be expressed for an asymmetric model, Figure 1a, as:

$$dV = \pi D_o N_T (Q/d)_a (P_h - P_l) dl \tag{1}$$

where $(Q/d)_a$ is called the specific permeability for the species in the asymmetric model. The value of d is not separately available in this model.

For a homogeneous model, the corresponding equation is:

$$dV = \pi D_{LM} N_T (Q_h/d_h)(P_h - P_l) dl \tag{2}$$

where

$$D_{LM} = (D_o - D_i)/\ln (D_o/D_i) \tag{3}$$

Q_h is the permeability in the homogeneous membrane model, and d_h is the actual physical thickness of the membrane. A comparison of Eqs. 1 and 2 indicates that:

$$D_o (Q/d)_a = D_{LM} (Q_h/d_h) \tag{4}$$

It means that the permeability values estimated from the experimental permeation data will be different for the two models. It does not matter, however, since all the governing equations for the asymmetric model will contain the product $D_o(Q/d)_a$, and all those for the homogeneous model will contain the product $D_{LM}(Q_h/d_h)$. Equality of these two products will therefore constitute the correct basis for comparing the two models.

In case of permeation separation from gas mixtures, component balance equations analogous to Eqs. 1 and 2 can be written. For a binary system with components 1 and 2 and with countercurrent flow of feed and sweep, the dimensionless forms of these equations are (Walawender and Stern, 1972; Pan and Habgood, 1978; Pan, 1983; Sengupta and Sirkar, 1986):

Permeation equations

Asymmetric membrane model

$$d(L^*x)/dl^* = K_1 \alpha (x - \gamma y') \tag{5}$$

$$d[L^*(1 - x)] = K_1 \alpha [1 - x - \gamma (1 - y')] \tag{6}$$

Homogeneous membrane model

$$d(L^*x)/dl^* = K_1 \alpha (x - \gamma y) \tag{7}$$

$$d[L^*(1 - x)] = K_1 \alpha [1 - x - \gamma (1 - y)] \tag{8}$$

where:

$$\begin{aligned} K_1 &= \pi D_o l_m N_T P_f (Q/d)_{a,2}/L_f \text{ (asymmetric model)} \\ &= \pi D_{LM} l_m N_T P_f (Q_h/d_h)_2/L_f \text{ (homogeneous model)} \end{aligned} \tag{9}$$

$$\begin{aligned} &l^* = l/l_m;\ L^* = L/L_f;\ V^* = V/L_f;\ \gamma = p/P_f; \\ &\alpha = (Q/d)_1/(Q/d)_2 \end{aligned} \tag{10}$$

In the feed-outside mode, P_f, the feed inlet pressure, can be taken as a constant, whereas the permeate pressure p (and hence γ) varies along the fiber length. The value of K_1 will be the same irrespective of the model because of Eq. 4. The difference between the two models lies in the use of y' in the driving force

expression $(x - \gamma y')$ where y' is based on crossflow in the porous backing (Pan, 1983):

$$y' = \alpha(x - \gamma y')/[\alpha(x - \gamma y') + (1 - x) - \gamma(1 - y')] \quad (11)$$

A mass balance of the more permeable species leads to

$$d(L^*x)/dl^* = d(V^*y)/dl^* \quad (12)$$

A similar balance may be written for the less permeable species.

It is more convenient to write an overall mass balance as

$$dL^*/dl^* = dV^*/dl^* \quad (13)$$

From Eqs. 5, 6, 12, and 13 one can get Eqs. 14–17

$$dx/dl^* = K_1\{\alpha(1 - x)(x - \gamma y') - x[1 - x - \gamma(1 - y')]\}/L^* \quad (14)$$

$$dy/dl^* = K_1\{\alpha(1 - y)(x - \gamma y') - y[1 - x - \gamma(1 - y')]\}/V^* \quad (15)$$

$$dL^*/dl^* = K_1[\alpha(x - \gamma y') + 1 - x - \gamma(1 - y')] \quad (16)$$

$$dV^*/dl^* = K_1[\alpha(x - \gamma y') + 1 - x - \gamma(1 - y')] \quad (17)$$

For the homogeneous model, the above equations will also apply with y' replaced by y.

The fiber lumen pressure drop is governed by:

$$d\gamma/dl^* = -K_2V^*/\gamma \quad (18)$$

where

$$K_2 = 128\,\mu\,R_gTl_mL_f/(\pi D_i^4N_TP_f^2) \quad (19)$$

Solving Eqs. 14–18 with the right boundary conditions, one can predict the permeator performance in terms of stage cut and feed/permeate outlet compositions.

It should be noted that all the above equations are valid whether one uses a sweep gas or not. The difference between a sweep mode and a no-sweep mode lies only in the boundary conditions. In the no-sweep mode, the bulk permeate mole fraction of the more permeable species, y, at the reject end cannot be specified and is related to the reject mole fraction and the closed end permeate pressure ratio according to the crossflow pattern existing at this particular location (Pan and Habgood, 1974).

In both sweep and no-sweep modes, since there is no permeation through the potted length of the fibers at the permeate end, integration of Eq. 18, will provide the appropriate boundary conditions of γ at the end of the active fiber length (Pan and Habgood, 1978; Sengupta and Sirkar, 1987).

No-sweep mode:

At $1^* = 0$

$$V^* = 0 \quad (20a)$$

$$y = \frac{1 + (\alpha - 1)(x + \gamma) - \{[1 + (\alpha - 1)(x + \gamma)]^2 - 4\alpha(\alpha - 1)\gamma x\}^{1/2}}{2(\alpha - 1)\gamma} \quad (20b)$$

At $1^* = 1$

$$x = x_f; \qquad L^* = 1 \quad (21a)$$

$$\gamma = [\gamma_o^2 + 2K_2V_{T1}^*(l_p/l_m)]^{1/2} \quad (21b)$$

Sweep mode:

At $1^* = 0$

$$V^* = Q_S/L_f; \qquad y = 0 \quad (22)$$

At $1^* = 1$

$$x = x_f; \qquad L^* = 1 \quad (23a)$$

$$\gamma = [\gamma_o^2 + 2K_2V_{T2}^*(l_p/l_m)]^{1/2} \quad (23b)$$

It is important to note that if one uses a sweep gas in the permeate side, the value of y, the bulk permeate composition, will be different from a no-sweep condition. Therefore the local permeation driving force $K_1\alpha(x - \gamma y)$ for the homogeneous membrane model will also be different. But the value of y' does not change because of the presence of sweep since, by definition, permeation in an asymmetric membrane is unaffected by the downstream compositions. Thus, the difference in the local driving force between the two models, which is equal to $K_1\alpha(\gamma y' - \gamma y)$, can be magnified to a great extent by using a sweep gas. The higher the sweep flow rate, the lower should be the value of y, and the higher should be the magnitude of $(y' - y)$. This will result in a substantial difference in the overall permeator performance as predicted by the two models.

Note the following points:

1. The sweep gas used is the less permeable feed component (N_2 for N_2-CO_2 system), and the system operating parameters are selected such that the highest N_2 partial pressure in the permeate side is less than the lowest N_2 partial pressure in the shell (feed) side.

2. This type of sweep gas method is preferred over the use of a third, "foreign" component, since it limits the present study to a binary separation scheme; the use of a foreign component will lead to the study of a ternary separation scheme because the permeation of this third species to the feed side introduces additional complexities.

3. The value of γ at any location in the permeator will depend weakly on the model since permeation and the pressure drop are affected by the model.

Feed-inside mode/tube-side feed

The basic difference here is that feed gas undergoes pressure drop, but permeate pressure is constant. Equations similar to Eqs. 7, 8, 12, and 13 can be developed:

$$d(L^*x)/dl^* = K_1\alpha(\Phi x - \gamma_p y) \quad (24)$$

$$d[L^*(1 - x)]/dl^* = K_1\alpha[\Phi(1 - x) - \gamma_p(1 - y)] \quad (25)$$

$$d(L^*x)/dl^* = d(V^*y)/dl^* \quad (26)$$

$$dL^*/dl^* = dV^*/dl \quad (27)$$

Here K_1 is based on D_{LM}, and Φ and γ_p are given as:

$$\Phi = P/P_f; \qquad \gamma_p = p_p/P_f \tag{28}$$

Further, Φ is the variable dimensionless feed pressure, and γ_p is the constant dimensionless permeate pressure.

From Eqs. 24–27 one can get the following equations:

$$dx/dl^* = -K_1\{\alpha(1-x)(\Phi x - \gamma_p y) - x[\Phi(1-x) - \gamma_p(1-y)]\}/L^* \tag{29}$$

$$dy/dl^* = -K_1\{\alpha(1-y)(\Phi x - \gamma_p y) - y[\Phi(1-x) - \gamma_p(1-y)]\}/V^* \tag{30}$$

$$dV^*/dl^* = dL^*/dl^* = -K_1 \cdot [\alpha(\Phi x - \gamma_p y) + \Phi(1-x) - \gamma_p(1-y)] \tag{31}$$

Also,

$$d\Phi/dl^* = -K_2 L^*/\Phi \tag{32}$$

The boundary conditions of the above set of governing equations are as follows:

At $l^* = 0$

$$x = x_f, L^* = 1 \quad \text{and} \quad \Phi = [1 - 2K_2(l_p/l_m)]^{1/2} \tag{33}$$

At $l^* = 1$

$V^* = 0$,

$$y = \frac{(\alpha-1)(\gamma_p + \Phi x) + \Phi - \{[(\alpha-1)(\gamma_p + \Phi x) + \Phi]^2 - 4\alpha(\alpha-1)\gamma_p \Phi x\}^{1/2}}{2\gamma_p(\alpha-1)} \tag{34}$$

Numerical technique

The set of coupled ordinary differential equations governing each model were solved on a DEC 10 mainframe computer. The split boundary value problems were solved using the IMSL routine DVCPR, which is based on a finite-difference algorithm (Pereyra, 1978). The initial estimates of each of the dependent variables, to be supplied when using IMSL routine DVCPR, were generated in the following fashion.

By considering cocurrent or crossflow configuration and no pressure drop through the fiber lumen, the problem is reduced to an initial-value problem that is solved easily using a fourth-order Runge-Kutta method. The obtained dependent variable profiles served as initial estimates for the actual boundary-value problem to be solved by IMSL routine DVCPR. These estimates were updated continuously by each iteration until the set of differential equations and the boundary conditions were solved subject to the prescribed tolerance. This procedure eliminates convergence problems and was first developed by Sengupta (1985). Details are available in papers by Sengupta and Sirkar (1984, 1987) and Majumdar et al. (1987).

Experimental Equipment and Procedure

The CA hollow fibers (of unknown degree of acetylation) were prepared from fibers used for reverse osmosis. A batch of wet fibers, taken from a Dow reverse osmosis module suitable for water desalination (Permutit Co., Paramus, NJ, model 96-05), was solvent-treated and dried according to the technique described by MacDonald and Pan (1974). Details are available in Sengupta (1985). The permeator was prepared by potting 70 such dried fibers in a 0.64 cm stainless steel tube, which acted as a shell, with male run tee end connections. The geometric characteristics of the permeator are given in Table 1. Two such permeators were built.

Table 1. Geometrical Characteristics of the Permeators

	Permeator 1	Permeator 2
No. CA fibers	70	70
Fiber OD, cm	2.3×10^{-2}	2.3×10^{-2}
Fiber ID, cm	0.84×10^{-2}	0.84×10^{-2}
Fiber active length, cm	63.8	63.98
Potted length, cm	2.4	2.4
Total membrane permeation area, cm^2	322.7	323.6
Shell ID, cm	0.48	0.48
Membrane area per unit shell volume, cm^{-1}	28	28
Packing fraction	0.16	0.16

In the feed-outside operation mode, as shown in Figure 1a, the high-pressure feed was introduced into and taken out of the shell. The permeate was collected from inside the fibers. In experiments with a sweep gas, the sweep was introduced into one end of the permeator and passed through the fiber bore, taking the permeate along with it. In runs without any sweep gas, the sweep inlet end was kept plugged and the permeate was withdrawn from the other end. In the feed-inside operation mode, the high-pressure feed passed through the fiber lumen and the permeate was withdrawn from the shell as shown in Figure 1b. The sweep gas used was pure nitrogen.

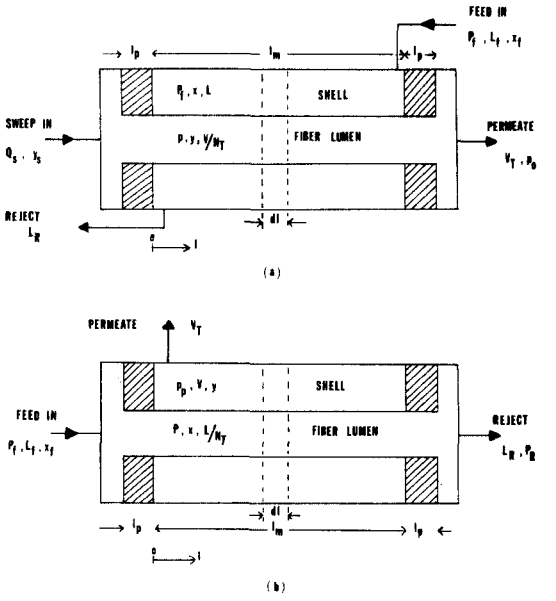

Figure 1. Membrane permeator configurations.
(a) Feed-outside mode/shell-side feed
(b) Feed-inside mode/tube-side feed

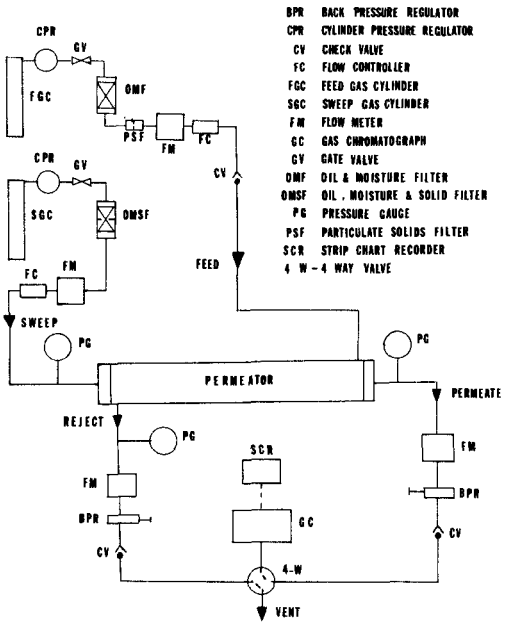

Figure 2. Experimental setup, feed-outside mode.

The permeation and separation runs in the feed-outside mode were carried out in the experimental apparatus shown schematically in Figure 2. This experimental setup consisted of the following gas lines: feed, reject, permeate, and when applicable, sweep inlet. The permeator module was kept at 25°C in a constant-temperature water bath. Feed gas of known composition was introduced at a controlled flow rate into the permeator. The feed line consisted of an oil-moisture filter, a digital flow transducer (Matheson, series 8141), a flow controller (Matheson, series 8241), and a particulate solids filter. The feed gas pressure was adjusted by a backpressure regulator (Fairchild Co., Salem, NC) in the reject line.

The sweep inlet gas line was connected to the permeator through a flow transducer (Matheson, series 8141), a flow controller (Matheson, series 8241), and a pressure gauge. In each of the reject and permeate lines there were a pressure gauge, a digital Matheson flow transducer, a backpressure regulator, and a check valve (C-series, Nupro Co., Willoughby, OH). The feed and sweep flow rates into the permeator were monitored and controlled by a multichannel read-out/control box (Matheson, model 8249).

A four-way valve (Whitney Co., Highland Heights, OH) was used to switch the reject and permeate streams to a gas chromatograph (model 1420, Varian, Walnut Creek, CA) with a thermal conductivity detector. A CTR column (catalog number 8700, Alltech, Deerfield, IL) with an inner packing of Porapak N and an outer packing of activated molecular sieve was used. The carrier gas was helium. All gases were supplied by Matheson, E. Rutherford, N.J.

The pure-component permeation experiments, which were needed to determine the individual specific permeabilities, were also carried out in the setup described above. In these experiments the reject line was plugged after the pressure gauge. The shell was pressurized with the pure gas under consideration. At steady state, the total rate of gas permeation through the walls of the hollow fibers was measured at the permeate outlet. The permeability measurements yielded individual specific permeabilities as a function of the feed (shell) pressure. For separation experiments, flow rates were measured and compositions of the permeate and reject streams were determined. At a given feed pressure, different stage cuts were achieved by varying the feed flow rates.

The simplified diagram shown in Figure 1b represents the permeator module operating in the feed-inside mode. In this case the feed was introduced at one end of the permeator and passed through the fiber lumen. The reject and permeate were collected from the opposite permeator end and the shell side, respectively. The nature of the instrumentation used in these three lines (feed, permeate, and reject) was essentially similar to that in the feed-outside mode. The feed-in and feed-out (reject) pressures were measured by different pressure gauges.

For pure-component permeability measurements in the feed-inside mode, the reject line was plugged just after the pressure gauge. The fiber lumina were pressurized with the pure gas under consideration. When the steady state was achieved, the total rate of gas permeation as measured by the flow in the shell outlet was determined. The inlet and closed end feed pressures were noted. For separation runs in the feed-inside mode, the stage cut variation at a given feed inlet pressure was achieved by varying the feed flow rate and measuring the corresponding flow rates and compositions of the permeate and reject streams.

Results and Discussion

The specific permeabilities of O_2, N_2, and CO_2 obtained from the feed-outside permeation experiments conducted at 25°C in permeators 1 and 2 are presented in Figure 3. In the calculation of the pure-component specific permeabilities the CA hollow fibers are assumed to be homogeneous in structure. When the membrane is assumed to be asymmetric, the corresponding specific permeabilities are obtained by converting the above permeabilities using Eq. 4. The figure shows that the pure-component specific permeabilities are essentially constant over the pressure range studied. It should be noted that the pure-component specific permeabilities measured in permeator 2 are 8% lower than those measured in permeator 1. These deviations could be attributed to property variations in different fiber batches.

Results of binary separation (CO_2-N_2) carried out in permea-

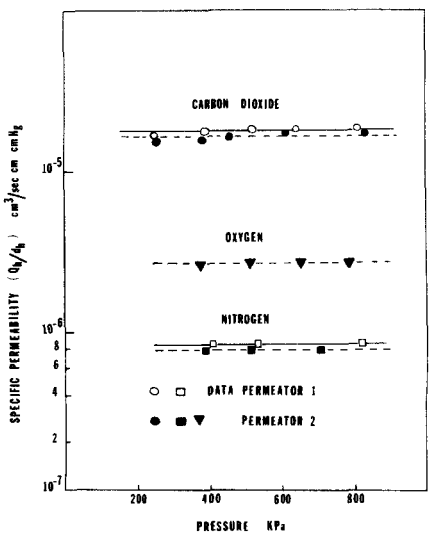

Figure 3. Specific permeabilities, feed-outside mode.

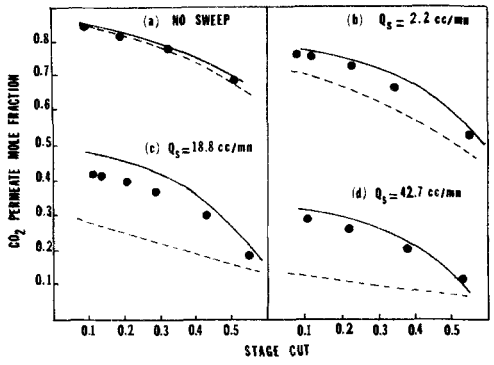

Figure 4. Separation in permeator 1, experiments vs. simulations.

Feed = 40% CO_2, 60% N_2; P_f = 404 kPa; γ_o = 0.25; y_s = 0.0
● Data; ——— Homogeneous model; ---- Asymmetric model

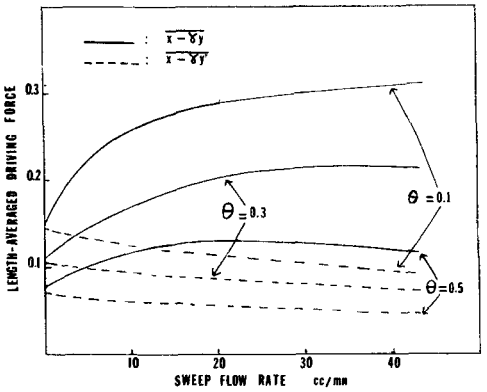

Figure 5. Effect of sweep flow rate on length-averaged driving forces in permeator 1, simulation only.

tor 1 with and without N_2 sweep in the feed-outside mode are indicated in Figure 4. The stage cut (defined as the fraction of the feed that has permeated) and the permeate mole fraction of the more permeable species (CO_2), are plotted against each other for four different sweep flow rates. The experimental data are compared to the corresponding values predicted by simulation. Two mathematical models were used, one assuming that the CA hollow fiber is symmetric (homogeneous) in structure, the other assuming that it is asymmetric.

Figure 4a shows the experimental data points and the simulation results for the no-sweep mode. We observe that the difference between the two proposed models is not large enough to let us conclude whether the CA hollow-fiber membrane behaves as an asymmetric or a homogeneous one (Sengupta and Sirkar, 1987).

One can substantially increase the difference between these two models by introducing a sweep gas. The effect of such a technique is shown in Figures 4b, c, d for three different sweep flow rates. It is seen that the experimental data points fall in between the homogeneous and asymmetric models. Further, it is evident that the homogeneous model predictions are much closer to the data than the asymmetric model predictions.

The length-averaged driving forces for the homogeneous and asymmetric models are $(\overline{x-\gamma y})$ and $(\overline{x-\gamma y'})$, respectively. These are direct measures of the rate of permeation of the more permeable component and are defined as follows:

$$\overline{x-\gamma y} = \int_0^1 (x-\gamma y)\,dl^* \tag{35a}$$

$$\overline{x-\gamma y'} = \int_0^1 (x-\gamma y')\,dl^* \tag{35b}$$

These two driving forces are plotted in Figure 5 as a function of the sweep flow rate for three different stage cuts. As the sweep flow rate increases, the pressure drop inside the fibers increases and at the same time the bulk permeate mole fraction of the more permeable species decreases. The decrease in y value much more than offsets the increase of γ and therefore as the sweep flow rate increases, the homogeneous length-averaged driving force $\overline{x-\gamma y}$ increases. On the other hand, the value of y' is not affected by the sweep flow rate. But as the sweep flow rate increases, the value of γ increases and therefore $\overline{x-\gamma y'}$ decreases.

Note first the negligible difference between the driving forces in the no-sweep mode (the difference between the corresponding y intercepts) due to the low value of the pressure ratio. This explains why there is not much difference between the two simulations shown in Figure 4a. It should also be noted that the $\overline{x-\gamma y}$ curve increases with the sweep flow rate and then reaches an asymptotic value for each of the three stage cuts. On the other hand, the $\overline{x-\gamma y'}$ curve first decreases as the sweep flow rate increases but then remains practically flat for most of the sweep flow rate range. However, the difference between the two models keeps on increasing with the sweep flow rate.

To test if some of the results obtained are generally valid, the following experiments were done. First, the separation data were checked with a different batch of fibers in permeator 2. Second, some of the experiments were repeated at a high feed pressure level, 1,480 kPa, (thereby increasing the permeation flux) with CO_2-N_2 gas mixture to see if the "in-between" behavior would still be observed at this high pressure level. Finally, separation experiments were carried out on the O_2-N_2 (air) system, which is a low separation factor system, as opposed to CO_2-N_2, which is a high separation factor system.

In Figure 6 we compare the experimental air separation performance with the homogeneous and asymmetric models under no-N_2 sweep conditions. It is apparent that for the two pressure levels studied, 501 and 708 kPa, the experimental data points are in between the two proposed models. Again, it is not possible to conclude which model fits the data better.

Figure 7 shows the CO_2-N_2 separation at a higher feed pressure with and without N_2 sweep. The y_{CO_2} vs. θ plots in this figure confirm the following: first, in the no-sweep mode it is not possible to conclude which model performs better; second, the homogeneous model in the sweep mode is closer to the data than

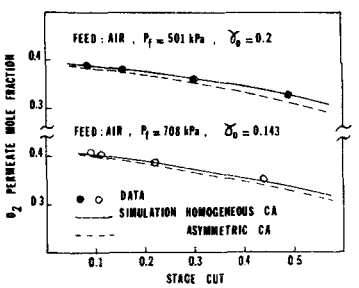

Figure 6. Air separation in permeator 2, experiments vs. simulations.

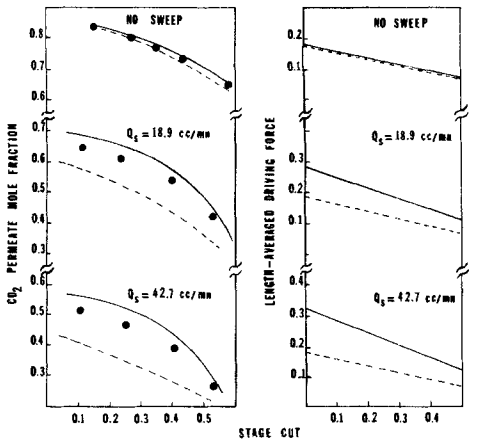

Figure 7. CO_2 permeate mole fraction and length-averaged driving force vs. stage cut for CO_2-N_2 separation in permeator 2.

Feed = 40% CO_2, 60% N_2; P_f = 1,480 kPa; γ_o = 0.25; y_s = 0.0
● Data; ——— Homogeneous model; --- Asymmetric model

the asymmetric model. This provides a justification for some earlier membrane stage analysis where asymmetric CA membrane was modeled for convenience as a homogeneous membrane (Chern et al., 1985). Further, it is also shown that as the sweep flow rate increases, the difference between the homogeneous and asymmetric length-averaged driving forces increases.

Table 2 compares the difference between the experimental and calculated permeate mole fraction of the more permeable component (CO_2) in terms of percent deviation defined by:

$$D_H = \frac{y_{HOM} - y_{EXP}}{y_{EXP}} \cdot 100 \qquad (36)$$

$$D_A = \frac{y_{ASY} - y_{EXP}}{y_{EXP}} \cdot 100 \qquad (37)$$

for the homogeneous and asymmetric models, respectively. This table compares the data obtained from the CO_2-N_2 separation at low and high pressure, 404 and 1,480 kPa, with the same sweep flow rate. In both cases the following is observed:

1. The homogeneous model always overpredicts with respect to the actual data, while the asymmetric model always underpredicts
2. The percent deviation for the homogeneous model, D_H, is almost the same irrespective of the stage cut and feed pressure
3. The homogeneous model predicts the experimental data much better than the asymmetric model

The table shows that as the feed pressure is decreased, the deviation from the asymmetric model, D_A, increases. This is understandable since as the feed pressure is lowered, the permeation rate decreases, and at the same sweep flow rate the net result is a greater dilution of the more permeable component in the permeate.

The mathematical model of the asymmetric membrane is valid only if the porous supporting layer has negligible resistance and if Knudsen diffusion along the pore path is insignificant compared to the high permeate flux. The specific permeabilities of the species studied in this work through the asymmetric membrane are quite low. And as mentioned by Pan (1983), an asymmetric membrane with low permeate flux may behave like a symmetric membrane due to the effect of back-diffusion along the pore path, which renders the local permeate composition y' close to that of the bulk permeate stream inside the fiber lumen. Sirkar's (1977) theoretical analysis of permeation through an asymmetric membrane anticipated this limit when the membrane skin resistance became high.

Gas separation by permeation through homogeneous hollow-fiber membranes with the feed flowing inside the fiber bore has been investigated by Blaisdell and Kammermeyer (1973) (silicone capillaries) and Pan and Habgood (1978). The latter have shown that the feed-inside operation mode is advantageous for high stage cuts when compared to the normal (feed-outside) operation mode. Since the present fibers appear to behave essentially as homogeneous membranes in the pressure range studied, it is logical to find out if separation can be achieved when the feed flows inside the fibers.

Permeability measurements in the feed-inside mode were car-

Table 2. Permeate Mole Fraction: Deviation of Experimental Values from Predictions of Homogeneous and Asymmetric Models

Stage Cut	Deviation, % D_H	Deviation, % D_A
P_f = 1,480 kPa, τ_o = 0.25, Q_s = 18.9 cm³/min Feed: 40% CO_2, 60% N_2; Sweep: N_2		
0.119	7.06	−10.74
0.238	8.47	−13.68
0.40	8.12	−19.19
0.531	8.57	−18.57
P_f = 404 kPa, τ_o = 0.25, Q_s = 18.7 cm³/min Feed: 40% CO_2, 60% N_2; Sweep: N_2		
0.101	7.98	−38.03
0.128	9.09	−38.76
0.209	9.55	−41.71
0.351	7.96	−43.75
0.545	10.87	−28.26

D_H, deviation from homogeneous model, Eq. 36
D_A, deviation from assymetric model, Eq. 37

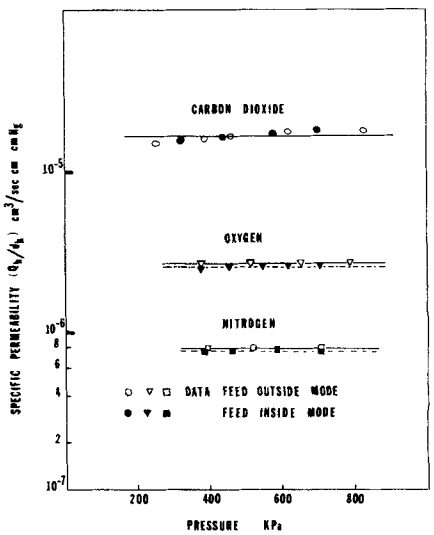

Figure 8. Specific permeabilities in permeator 2.

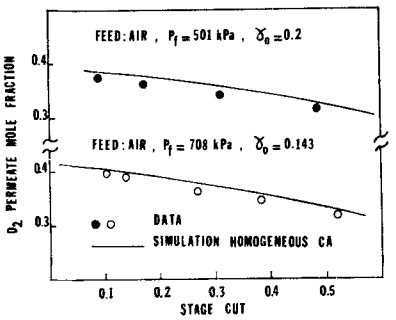

Figure 9. Air separation in permeator 2, feed-inside mode; experiments vs. simulations.

ried out to compute the specific permeabilities for each species: O_2, N_2, and CO_2. In computing these permeabilities, plotted in Figure 8, the CA fiber was assumed to be homogeneous in structure. The plot shows:

1. The permeabilities in the feed-inside mode are independent of pressure
2. They are almost identical to the permeabilities in the feed-outside mode

Figure 9 shows the experimental data and simulation results for air separation in the feed-inside mode carried out at two different feed inlet pressures, 501 and 708 kPa. These plots show that the assumed homogeneous model fits the data well. It indicates that the homogeneous model is probably a better choice since in both feed-in and feed-out modes it predicts the experimental data well. It also indicates that there is little concentration polarization effect present in the porous substrate of the CA fibers. Had such an effect been present, the simple homogeneous membrane model would not have been able to predict the data so well.

However, in order to investigate thoroughly the effect of concentration polarization with the actual membrane, one should conduct a study with a highly permeable species. It is believed that under high-flux conditions, significant concentration polarization is likely to occur with asymmetric membranes.

Figure 10 compares the experimental performance of the hollow-fiber permeator operated in the feed-outside and feed-inside modes. The results indicate that for a given stage cut and under the same operating conditions, the permeator performs marginally better in the feed-outside mode. It should be remembered that the comparative performance may change under different operating conditions.

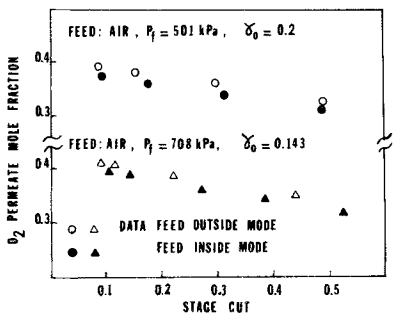

Figure 10. Air separation in permeator 2, experimental operation in feed-outside and feed-inside modes.

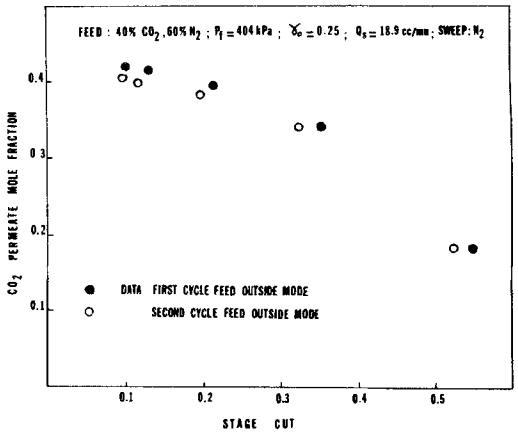

Figure 11. Hysteresis effect on gas separation through asymmetric CA fibers.

Lastly, we check if there is any hysteresis-type performance loss in the membrane upon internal pressurization. In Figure 11, filled circles correspond to the first binary separation runs (CO_2-N_2) carried out in permeator 2 in the feed-outside mode. Once the first set of feed-outside experiments was over, the permeator was operated for a while (more than 400 h) in the feed-inside mode. Upon completion of this latter mode of operation, the permeator was subjected to a second set of feed-outside mode experiments. The corresponding data, represented by open circles in Figure 11, show that there is no significant loss of performance during the feed-outside/feed-inside cycle for the pressure range studied.

Conclusions

A sweep gas technique has been introduced to enhance considerably the difference between the homogeneous and asymmetric membrane models of asymmetric CA hollow fibers.

In the feed-outside mode, comparison of the data with the theoretical predictions shows that the homogeneous model, in the pressure range studied, fits the experimental behavior of the CA membrane better than the asymmetric model.

It is also shown that the homogeneous model fits the data fairly well when the permeator is operated in the feed-inside mode. Further, the permeator performance is relatively unaffected by the mode of feed operation (feed outside or feed inside).

It has also been shown that for the low-pressure range studied, there is essentially no hysteresis behavior when operation is switched between the feed-outside and feed-inside modes.

Finally, it should be realized that since there are various kinds of asymmetric CA hollow fibers, generalizations are difficult to reach from the results of the present study. With asymmetric CA hollow fibers having a much thinner dense skin, the backing resistance at high flux levels may influence the behavior much more than observed here.

Notation

D_i, D_o = inside, outside diameter of cellulose acetate fibers, m
D_{LM} = logarithmic mean of inside and outside diameters of cellulose acetate, Eq. 3, m
K_1, K_2 = constants, Eqs. 9, 19

l = distance, m
l_m = total effective length of permeation, m
l_p = potted length of cellulose acetate fibers, m
l^* = dimensionless distance, Eq. 10
L = local feed flow rate, mol/s
L_f = feed flow rate at permeator entry, mol/s
L_R = reject flow rate, mol/s
L^* = dimensionless local feed flow rate, Eq. 10
N_T = total number of cellulose acetate fibers
p = local permeate pressure in feed-outside mode, Pa
p_o = permeate pressure at open end of cellulose acetate fibers, feed-outside mode, Pa
P = local feed pressure in feed-inside mode, Pa
P_h = high-pressure side
P_l = low-pressure side
p_p = permeate pressure in feed-inside mode, Pa
P_f = inlet feed pressure, Pa
$(Q/d)_i$ = specific permeability of species i, mol/s · m^2 · Pa
$(Q/d)_{a,i}$ = specific permeability of species i for asymmetric membrane model, mol/s · m^2 · Pa; i = 1, more permeable species
$(Q_h/d_h)_i$ = specific permeability of species i for homogeneous membrane model, mol/s · m^2 · Pa; i = 1, more permeable species
Q_s = sweep flow rate, mol/s
R_g = universal gas constant, Pa · m^3/mol · K
T = absolute temperature, K
V = local permeate flow rate, mol/s
V^* = normalized value of V, Eq. 10
V_{T1^*} = normalized value of V at permeate end, sweep mode
V_{T2^*} = normalized value of V at permeate end, sweep mode
x = local mole fraction of more permeable component on feed side
x_f = value of x at feed entry
y = local mole fraction of more permeable component on permeate side
y' = local value of permeate mole fraction of more permeable component, based on local crossflow, Eq. 11
y_{ASY} = permeate mole fraction of more permeable component predicted by asymmetric model
y_{EXP} = permeate mole fraction of more permeable component determined experimentally
y_{HOM} = permeate mole fraction of more permeable component predicted by homogeneous model
y_s = sweep mole fraction of more permeable component

Greek letters

α = ideal separation factor, Eq. 10
γ = local pressure ratio, Eq. 10
γ_o = value of γ at permeate outlet
γ_p = pressure ratio, Eq. 28
θ = stage cut
μ = gas viscosity, Pa · s
π = 3.14159 . . .
Φ = local dimensionless feed pressure, Eq. 28

Literature Cited

Antonson, C. R., R. J. Gardner, C. F. King, and D. Y. Ko, "Analysis of Gas Separation by Permeation in Hollow Fibers," *Ind. Eng. Chem. Process Des. Dev.*, **16,** 463 (1977).

Blaisdell, C. T., and K. Kammermeyer, "Countercurrent and Cocurrent Gas Separation," *Chem. Eng. Sci.*, **28,** 1249 (1973).

Bollinger, W. A., D. L. MacLean, and R. S. Narayan, "Separation Systems for Oil Refining and Production," *Chem. Eng. Prog.*, **78,** 27 (1982).

Chern, R. T., W. J. Koros, and P. S. Fedkiw, "Simulation of a Hollow-Fiber Gas Separator: The Effects of Process Design Variables," *Ind. Eng. Chem. Process Des. Dev.*, **24,** 1015 (1985).

Henis, J. M. S., and M. K. Tripodi, "A Novel Approach to Gas Separations Using Composite Hollow-Fiber Membranes," *Sep. Sci. Technol.*, **15,** 1059 (1980).

Henis, J. M. S., and M. K. Tripodi, "Composite Hollow-Fiber Membranes for Gas Separation: The Resistance Model Approach," *J. Membrane Sci.*, **8,** 233 (1981).

MacDonald, W., and C. Y. Pan, "Method for Drying Water-Wet Membranes," U.S. Pat. 3,842,515 (1974).

Majumdar, S., L. B. Heit, A. Sengupta, and K. K. Sirkar, "An Experimental Investigation of Oxygen Enrichment in a Silicone Capillary Permeator with Permeate Recycle," *Ind. Eng. Chem. Res.*, **26,** 1434 (1987)

Mazur, W. H., and M. C. Chan, "Membranes for Natural Gas Sweetening and CO_2 Enrichment," *Chem. Eng. Prog.*, **78,** 38 (1982).

Mehta, G. D., and S. Loeb, "Internal Polarization in the Porous Substructure of a Semipermeable Membrane Under Pressure-Retarded Osmosis," *J. Membrane Sci.*, **4,** 261 (1978).

Pan, C. Y., "Gas Separation by Permeators with High-Flux Asymmetric Membranes," *AIChE J.*, **29,** 545 (1983).

———, "Gas Separation by High-Flux Asymmetric Hollow-Fiber Membrane," *AIChE J.*, **32,** 2020 (1986).

Pan, C. Y., and H. W. Habgood, "An Analysis of the Single-Stage Gaseous Permeation Process," *Ind. Eng. Chem. Fundam.*, **13,** 323 (1974).

———, "Gas Separation by Permeation. II: Effect of Permeate Pressure Drop and Choice of Permeate Pressure," *Can. J. Chem. Eng.*, **56,** 210 (1978).

Pereyra, V., "PASVA3: An Adaptive Finite-Difference FORTRAN Program for First-Order Nonlinear Ordinary Boundary Value Problems," *Lecture Notes on Computer Science,* Springer Verlag, Berlin, **76,** 67 (1978).

Perrin, J. E., and S. A. Stern, "Separation of a Helium-Methane Mixture in Permeation with Two Types of Polymer Membranes," *AIChE J.*, **32,** 1889 (1986).

Rautenbach, R., and R. Albrecht, "On the Behavior of Asymmetric Membranes in Pervaporation," *J. Membrane Sci.*, **19,** 1 (1984).

Schell, W. J., and C. D. Houston, "Spiral-wound Permeators for Gas Purification and Recovery," *Chem. Eng. Prog.*, **78,** 33 (1982).

Sengupta, A., "Investigations on Binary and Ternary Gas Separations Using Polymeric Membrane Permeators," Ph.D. Diss., Dept. Chem. and Chem. Eng., Stevens Inst. Technol., Hoboken, NJ (1985).

Sengupta, A., and K. K. Sirkar, "Multicomponent Gas Separation by an Asymmetric Permeator Containing Two Different Membranes," *J. Membrane Sci.*, **21,** 73 (1984).

———, "Membrane Gas Separation," *Progress in Filtration and Separation,* R. J. Wakeman, ed., v. 4, Elsevier, Amsterdam, 289 (1986).

———, "Ternary Gas Mixture Separation in Two-Membrane Permeators," *AIChE J.*, **33,** 529 (1987).

Sirkar, K. K., "Separation of Gaseous Mixtures with Asymmetric Dense Polymeric Membranes," *Chem. Eng. Sci.*, **32,** 1137 (1977).

Stern, S. A., F. J. Onorato, and C. Libove, "The Permeation of Gases Through Hollow Silicone Rubber Fibers: Effect of Fiber Elasticity on Gas Permeability," *AIChE J.*, **23,** 567 (1977).

Walawender, W. P., and S. A. Stern. "Analysis of Membrane Separation Parameters. II: Countercurrent and Cocurrent Flow in a Single Permeation Stage," *Separ. Sci.*, **7,** 553 (1972).

Yamashiro, H., M. Hirajo, W. J. Schell, and C. F. Maitland, "Hydrogen Purification with Cellulose Acetate Membranes," paper distributed at the Europe-Japan Cong. Membranes and Membrane Processes, Stressa, Italy (June, 1984).

Manuscript received Jul. 2, 1987, and revision received Sept. 23, 1987.